

# Measurement of the Shear Wavespeed in an Isotropic Elastomeric Plate

Andrew J. Hull  
Benjamin A. Cray  
Autonomous and Defensive Systems Department



20090113299

**Naval Undersea Warfare Center Division  
Newport, Rhode Island**

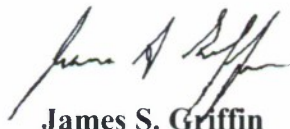
## **PREFACE**

This report was funded by the Office of Naval Research (ONR). This report was prepared under Project No. 03302, "Validating the Structural Acoustic Response of Elastomeric and 1-3 Piezoceramic Plates," principal investigator Dr. Benjamin A. Cray (Code 821).

The technical reviewer for this report was Jason M. Maguire (Code 1512).

The authors gratefully acknowledge Program Officer David M. Drumheller at ONR for his sponsorship. Additionally, the authors thank Walter H. Boober, Rene J. LaFleur, and Gorham G. Lau of the Naval Undersea Warfare Center's Acoustic Test Facility for the collection of spatial domain data.

**Reviewed and Approved: 10 October 2008**



**James S. Griffin**

**Head, Autonomous and Defensive Systems Department**



# REPORT DOCUMENTATION PAGE

Form Approved  
OMB No. 0704-0188

The public reporting burden for this collection of information is estimated to average 1 hour per response, including the time for reviewing instructions, searching existing data sources, gathering and maintaining the data needed, and completing and reviewing the collection of information. Send comments regarding this burden estimate or any other aspect of this collection of information, including suggestions for reducing this burden, to Department of Defense, Washington Headquarters Services, Directorate for Information Operations and Reports (0704-0188), 1215 Jefferson Davis Highway, Suite 1204, Arlington, VA 22202-4302. Respondents should be aware that notwithstanding any other provision of law, no person shall be subject to any penalty for failing to comply with a collection of information if it does not display a currently valid OPM control number.  
PLEASE DO NOT RETURN YOUR FORM TO THE ABOVE ADDRESS.

1. REPORT DATE (DD-MM-YYYY) 10-10-2008			2. REPORT TYPE Interim		3. DATES COVERED (From - To)	
4. TITLE AND SUBTITLE  Measurement of the Shear Wavespeed in an Isotropic Elastomeric Plate					5a. CONTRACT NUMBER	
					5b. GRANT NUMBER	
					5c. PROGRAM ELEMENT NUMBER	
6. AUTHOR(S)  Andrew J. Hull Benjamin A. Cray					5.d PROJECT NUMBER	
					5e. TASK NUMBER	
					5f. WORK UNIT NUMBER	
7. PERFORMING ORGANIZATION NAME(S) AND ADDRESS(ES)  Naval Undersea Warfare Center Division 1176 Howell Street Newport, RI 02841-1708					8. PERFORMING ORGANIZATION REPORT NUMBER  TR 11894	
9. SPONSORING/MONITORING AGENCY NAME(S) AND ADDRESS(ES)					10. SPONSORING/MONITOR'S ACRONYM	
					11. SPONSORING/MONITORING REPORT NUMBER	
12. DISTRIBUTION/AVAILABILITY STATEMENT  Approved for public release; distribution is unlimited.						
13. SUPPLEMENTARY NOTES						
14. ABSTRACT  A method to estimate the shear wavespeed in an isotropic, thick, elastomeric plate is demonstrated in this report. A point force is applied to the plate and a scanning laser vibrometer is used to measure normal velocity on one surface. The temporal domain measurements are transformed into the frequency domain using a Fourier transform, then, the spatial domain measurements are transformed into the $k_x, k_y$ wavevector domain using two Fourier transforms. Once the data are in the wavevector-frequency domain, the propagation wavenumbers for specific Lamb waves can be estimated from the peaks within the $k_x, k_y$ spectra. Using the estimated values of the propagation wavenumbers, a Newton-Raphson gradient method is applied to the Raleigh-Lamb dispersion curve equations to obtain an estimate of the shear wavespeed, a quantity that is generally difficult to measure. A simulation and an experiment are included to illustrate the method, and the accuracy of the measurement process is discussed.						
15. SUBJECT TERMS  Shear Wavespeed Measurement      Inverse Method						
16. SECURITY CLASSIFICATION OF:			17. LIMITATION OF ABSTRACT	18. NUMBER OF PAGES  33	19a. NAME OF RESPONSIBLE PERSON  Andrew J. Hull	
a. REPORT (U)	b. ABSTRACT (U)	c. THIS PAGE (U)			19b. TELEPHONE NUMBER (Include area code)  (401) 832-5189	

## TABLE OF CONTENTS

Section	Page
LIST OF TABLES .....	ii
1 INTRODUCTION .....	1
2 SYSTEM EQUATIONS .....	3
3 NUMERICAL SIMULATION .....	9
4 EXPERIMENT .....	15
5 CONCLUSIONS .....	21
APPENDIX A—MEASUREMENT OF DILATATIONAL WAVESPEED .....	A-1
APPENDIX B—COEFFICIENTS OF TRANSFER FUNCTION MATRICES .....	B-1
REFERENCES .....	R-1

## LIST OF ILLUSTRATIONS

Figure	Page
1 Frequency Equation (1) for the Propagation of Symmetric Waves in an Elastic Plate Versus Shear and Dilatational Wavenumber .....	5
2 Frequency Equation (2) for the Propagation of Antisymmetric Waves in an Elastic Plate Versus Shear and Dilatational Wavenumber .....	6
3 Locations in the Wavevector Plane for Simulation of F(0), L(0) and FE (1) Waves for 5 kHz (FE(1) Wave (o), L(0) Wave (+), F(0) Wave (x), and Least-Square Fit Circles ( ____ )) .....	13
4 Performance of Estimation Routine Versus Initial Estimate of Shear Wavespeed for Specific Wave Type and Frequency .....	13
5 Experimental Setup of the Shear Wave Estimation Test .....	17

## LIST OF ILLUSTRATIONS (Cont'd)

Figure	Page
6 Locations in the $k_x, k_y$ Wavevector Plane for Experiment of F(0), L(0) and FE(1) Waves for 5 kHz (FE(1) Wave (o), L(0) Wave (+), F(0) Wave (x), and Least-Square Fit Circles ( ____ )).....	17
7 Dispersion Curve of the Plate F(0) Wave Data (x), L(0) Wave Data (+), FE(1) Wave Data (o), and Theory ( ____ )) .....	18
A-1 Magnitude of the Echo Reduction for the Plate Under Investigation.....	A-2

## LIST OF TABLES

Table	Page
1 Estimated Shear Wavespeeds for Simulated Waves.....	12
2 Estimated Shear Wavespeeds for All Measured Waves .....	16
3 Statistical Analysis of Estimated Shear Wavespeeds .....	19
A-1 Dilatational Wavespeed Estimates at Relative Maxima .....	A-2



# MEASUREMENT OF THE SHEAR WAVESPEED IN AN ISOTROPIC ELASTOMERIC PLATE

## 1. INTRODUCTION

Measurement of material properties of elastic systems has been and continues to be an active area of investigation. Resonant techniques have been used<sup>1-4</sup> that usually involve measuring the natural resonant frequencies of slender structures. Once measured, these frequencies are equated to the corresponding analytical natural frequencies, which are typically functions of Young's modulus, shear modulus, length and/or mass. The resultant expression can be solved, which produces an estimate of Young's or shear modulus at each natural frequency. Nonresonant methods<sup>2,5,6</sup> have also been used. Although slightly more complicated than resonant techniques, these methods have the ability to estimate material properties at frequencies other than the natural frequency of the system. Typically, nonresonant techniques involve equating measured data with a simplified analytical model of the system. The analytical model is rewritten so that the material properties that are to be estimated are rendered as functions of the data.

Both resonant and nonresonant methods are usually performed at low frequencies, where simple (though limited) analytical models and corresponding dynamic behavior exists. Ideally, the structure under testing will have only a single mode of energy propagation, so that the effects of other wave motion will not corrupt the estimation process.

Few wavespeed estimation techniques have been developed for general plates and beams. Most of the research has assumed thin plate (or beam) behavior where the theory is that of a single flexural wave propagating in the structure. The estimation of Young's modulus and shear modulus have been accomplished by matching the theoretical eigenfrequencies of a Timoshenko beam model to measured data and then deducing the material parameters.<sup>7</sup> Some techniques at ultrasonic frequencies have been derived, frequently to support the medical imaging or the aviation industry. The measurement of elastic constants of thin immersed anisotropic plates has been undertaken using the identification of transmission zeros and poles based on various incident angles of an incoming ultrasonic wave.<sup>8</sup> The estimation of stiffness and damping

properties of viscoelastic materials by numerically inverting the transmitted ultrasonic field of an immersed thin plate at different incident angles has been accomplished.<sup>9</sup> A method has been devised to identify Lamé constants, thickness, density, longitudinal and shear attenuation and interfacial properties of a solid layer placed between two other layers.<sup>10</sup> This method uses normal and angular ultrasonic reflectivity from the middle layer. The last three references involve modeling and measurement in the MHz region. Many indentation material testing methods exist.<sup>11</sup> These usually consist of loading a location of the material and measuring the resultant force and depth. Using these measurements, one can determine Young's modulus and shear modulus. These methods are usually quasi-static and frequency independent.

The elastic plate theory has been extensively developed,<sup>12,13</sup> though thick plates have traditionally not been used to measure material properties because they support multiple wave types, and any measurement technique has to have the ability to discern between each wave type and its contribution to the measurement. Transfer function methods that measure one output (at a single location) versus a fixed input do not have the capability to separate various wave types and their associated response levels. It is precisely this property of multiple wave types that this report exploits to measure the shear wavespeed in a thick plate. This is in the region where dilatational and shear wavelengths begin to approach the plate thickness, i.e., fully elastic dynamic behavior. The plate is mechanically excited by a point force at a fixed frequency while simultaneously measuring the normal velocity of the plate across its entire surface. These spatial domain measurements are transferred into a wavevector (two-wavenumber  $(k_x, k_y)$ ) domain by means of two Fourier transforms. Individual waves are identified in this domain, and the resulting wave propagation wavenumbers are accurately estimated. Once they are measured, the estimated wavenumbers are inserted into a Newton-Raphson iterative solver applied to the theoretical Rayleigh-Lamb equations for the propagation of waves in a plate with traction-free boundary conditions. Results of estimates of the squares of the shear wavenumbers are thus obtained, allowing for calculations of the shear wavespeed. Numerical simulations are used to confirm accuracy. An experiment is completed and is included to illustrate and verify the technique. The first three Lamb waves propagating in a urethane plate are excited at several frequencies and the inverse method is applied. From this, estimates of the shear wavespeed are determined.

## 2. SYSTEM EQUATIONS

The theory of wave motion in isotropic elastic thick plates is extensively developed. The objective of this work is to estimate the shear wavespeed using the theoretical Rayleigh-Lamb equations developed for free-free plate boundary conditions. Free-free plate boundary conditions correspond to the case of traction-free boundaries; i.e., the normal and shear stresses at the plate faces are zero. There are two separate Rayleigh-Lamb dispersion equations based on the symmetry of the horizontal displacement field about the mid-plane of the plate; one corresponds to symmetrical waves and the other to antisymmetric waves. The Rayleigh-Lamb equation for the propagation of symmetric waves is written as<sup>12</sup>

$$f(k_d, k_s) = \frac{\tan[\sqrt{k_s^2 - k^2}(h/2)]}{\tan[\sqrt{k_d^2 - k^2}(h/2)]} + \frac{4k^2 \sqrt{k_d^2 - k^2} \sqrt{k_s^2 - k^2}}{(2k^2 - k_s^2)^2} = 0, \quad (1)$$

and the Rayleigh-Lamb equation for the propagation of antisymmetric waves is given by<sup>12</sup>

$$g(k_d, k_s) = \frac{\tan[\sqrt{k_s^2 - k^2}(h/2)]}{\tan[\sqrt{k_d^2 - k^2}(h/2)]} + \frac{(2k^2 - k_s^2)^2}{4k^2 \sqrt{k_d^2 - k^2} \sqrt{k_s^2 - k^2}} = 0, \quad (2)$$

where  $h$  is the thickness of the plate (m),  $k_s$  is the shear wavenumber ( $\text{rad m}^{-1}$ ),  $k_d$  is the dilatational wavenumber ( $\text{rad m}^{-1}$ ), and  $k$  is the propagation wavenumber ( $\text{rad m}^{-1}$ ). When equation (1) or (2) is satisfied, the propagation wavenumber  $k$  corresponds to a specific Lamb wave (sometimes also referred to as Rayleigh-Lamb wave) traveling in the plate. Note that equation (1) or (2) will be applicable to any specific wave in the plate, but not both. These two equations define the wavenumber-frequency dispersion curves and will be used with the identification of Lamb waves in the medium to estimate the shear wavespeed. The measurement or estimation of the propagation wavenumber of interest,  $k$ , is discussed in the next section. The relationship between shear wavenumber and shear wavespeed is



$$k_s = \frac{\omega}{c_s}, \quad (3)$$

where  $\omega$  is the angular frequency ( $\text{rad s}^{-1}$ ) and  $c_s$  is the shear wavespeed ( $\text{ms}^{-1}$ ). The relationship between dilatational wavenumber and dilatational wavespeed is

$$k_d = \frac{\omega}{c_d}, \quad (4)$$

where  $c_d$  is the dilatational wavespeed ( $\text{m s}^{-1}$ ).

To better understand the functions  $f(k_d, k_s)$  and  $g(k_d, k_s)$ , it is informative to display them as surfaces with respect to dilatational and shear wavenumber and examine their characteristic behavior. Figure 1 is a plot of the function  $f(k_d, k_s)$  versus shear and dilatational wavenumber using a propagation wavenumber of  $k = 68.9 \text{ rad m}^{-1}$  displayed using a decibel scale. Figure 2 is a plot of the function  $g(k_d, k_s)$  versus shear and dilatational wavenumber using a propagation wavenumber of  $k = 128.9 \text{ rad m}^{-1}$  displayed using a decibel scale. In both figures 1 and 2, the right plot is a plot of the function with respect to the dilatational wavenumber with the shear wavenumber fixed at  $100 \text{ rad m}^{-1}$ , and the bottom plot is a plot of the function with respect to the shear wavenumber with the dilatational wavenumber fixed at  $16 \text{ rad m}^{-1}$ . The plate thickness  $h$  was  $0.0254 \text{ m}$  and the frequency  $\omega$  was  $(2\pi)4000 \text{ rad s}^{-1}$ . Note that in both plots, the functions vary significantly with respect to the shear wavenumber and are essentially flat with respect to the dilatational wavenumber. This overarching feature reveals two pertinent dynamic characteristics, which guide the estimation process: (1) the shear wavenumber (and, hence, the shear wavespeed) can be accurately estimated due to the well-defined minimum values of the surface with respect to the shear wavenumber; and (2) the dilatational wavenumber will be poorly estimated using this method due to the poorly defined, slowly varying minimum values of the surface with respect to the dilatational wavenumber. The estimation of the shear wavenumber, within this region, is relatively invariant with respect to the dilatational wavenumber.

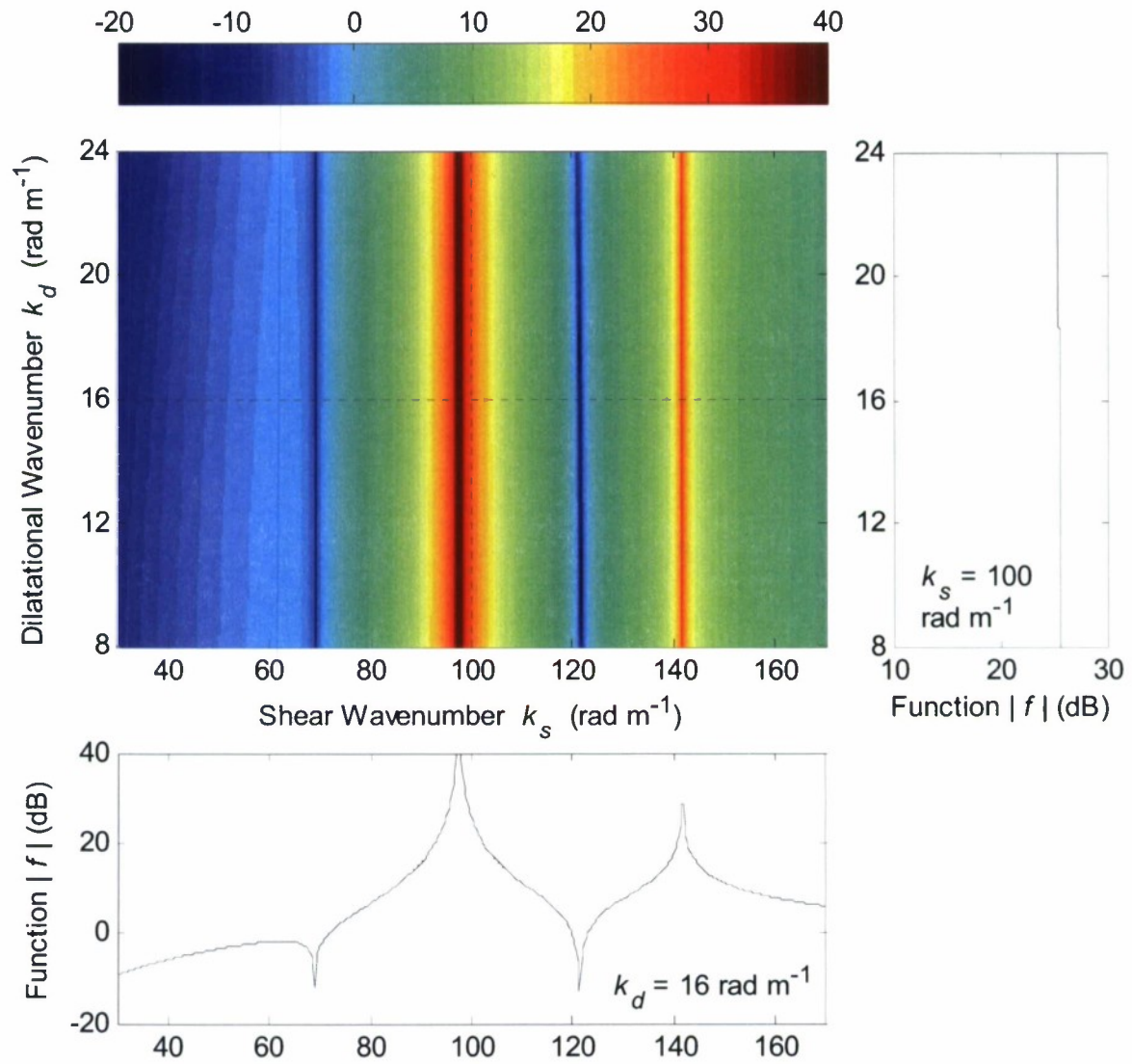


**Figure 1. Frequency Equation (1) for the Propagation of Symmetric Waves in an Elastic Plate Versus Shear and Dilatational Wavenumber**

(The right plot is with the shear wavenumber fixed at 100 rad m<sup>-1</sup>; the bottom plot is with the dilatational wavenumber fixed at 16 rad m<sup>-1</sup>. For all plots, propagation wavenumber is 68.9 rad m<sup>-1</sup> and frequency is 4 kHz.)

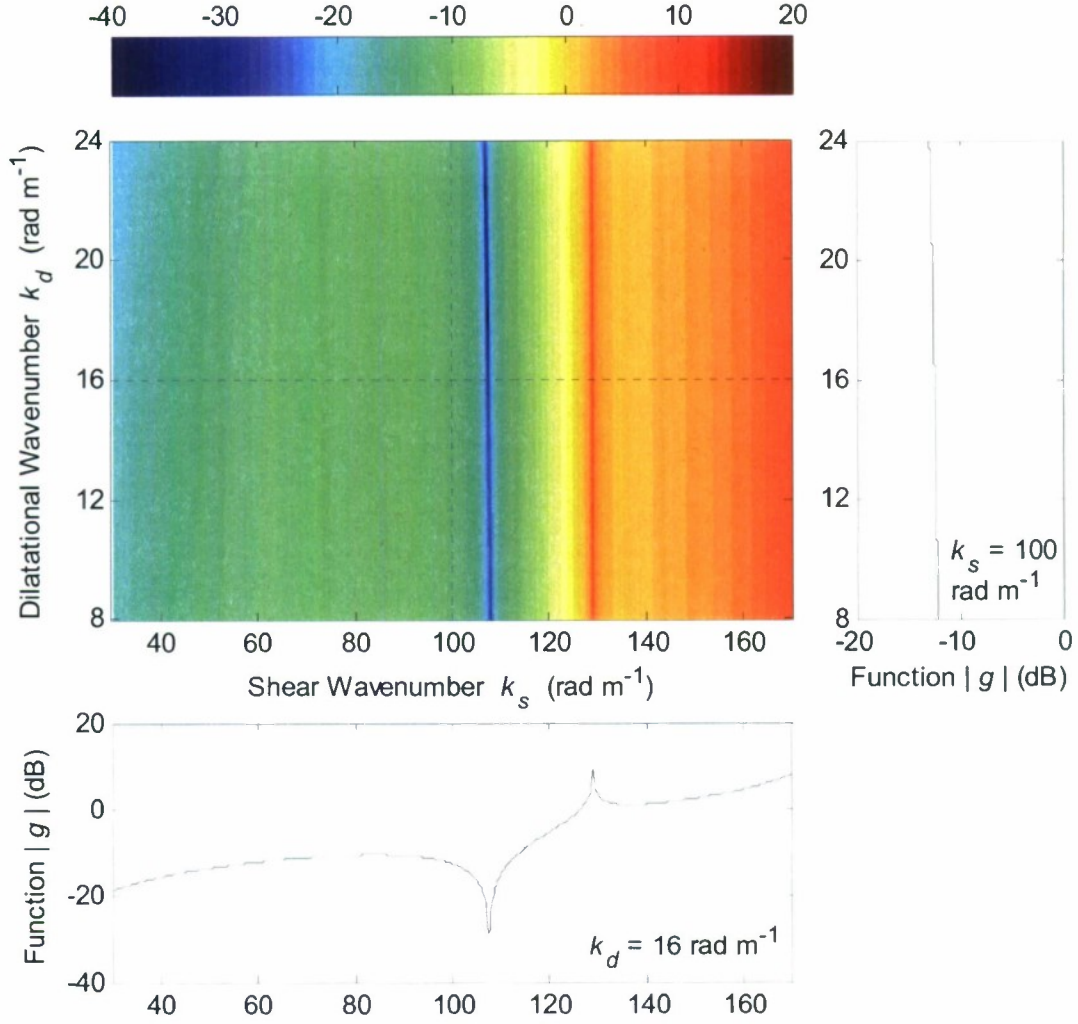


**Figure 2. Frequency Equation (2) for the Propagation of Antisymmetric Waves in an Elastic Plate Versus Shear and Dilatational Wavenumber**

(The right plot is with the shear wavenumber fixed at 100 rad m<sup>-1</sup>; the bottom plot is with the dilatational wavenumber fixed at 16 rad m<sup>-1</sup>. For all plots, the propagation wavenumber is 128.9 rad m<sup>-1</sup> and the frequency is 4 kHz.)

The dilatational wavespeed is assumed to be a known value and a convenient method to measure this wavespeed is given in appendix A. In section 4, it will be analyzed how an error in the dilatational wavespeed measurement will affect the shear wavespeed measurement. Using the dilatational wavespeed measured using the method described in appendix A, the dilatational wavenumber is calculated using equation (4). The propagation wavenumber is a known quantity that can be determined either from a simulation or via experiment (this is further discussed in sections 3 and 4). With both the dilatational wavenumber and the propagation wavenumber

known, a Newton-Raphson method<sup>14</sup> can then be applied to equations (1) or (2) for the estimation of the shear wavenumber that generates a value of zero for the function  $f(k_d, k_s)$  or  $g(k_d, k_s)$ . To eliminate the ambiguity of both positive and negative shear wavenumbers, the estimation process is applied to the square of the wavenumber, rather than the wavenumber itself. For equation (1) written as  $f(k_d, k_s) = 0$ , the Newton-Raphson method yields

$$\left[ k_s^2 \right]_{j+1} = \left[ k_s^2 \right]_j - \left[ \frac{\partial f(k_d, k_s)}{\partial (k_s^2)} \right]_j^{-1} f(k_d, k_s)_j, \quad (5)$$

where

$$\begin{aligned} \frac{\partial f(k_d, k_s)}{\partial (k_s^2)} = & \frac{h\{1 + \tan^2[\sqrt{k_s^2 - k^2}(h/2)]\}}{4\sqrt{k_s^2 - k^2} \tan[\sqrt{k_d^2 - k^2}(h/2)]} + \\ & \frac{2k^2 \sqrt{k_d^2 - k^2}}{\sqrt{k_s^2 - k^2} (2k^2 - k_s^2)^2} + \frac{8k^2 \sqrt{k_d^2 - k^2} \sqrt{k_s^2 - k^2}}{(2k^2 - k_s^2)^3}. \end{aligned} \quad (6)$$

For equation (2) written as  $g(k_d, k_s) = 0$ , the Newton-Raphson method yields

$$\left[ k_s^2 \right]_{j+1} = \left[ k_s^2 \right]_j - \left[ \frac{\partial g(k_d, k_s)}{\partial (k_s^2)} \right]_j^{-1} g(k_d, k_s)_j, \quad (7)$$

where

$$\begin{aligned} \frac{\partial g(k_d, k_s)}{\partial (k_s^2)} = & \frac{h\{1 + \tan^2[\sqrt{k_s^2 - k^2}(h/2)]\}}{4\sqrt{k_s^2 - k^2} \tan[\sqrt{k_d^2 - k^2}(h/2)]} + \\ & \frac{-(2k^2 - k_s^2)}{2k^2 \sqrt{k_d^2 - k^2} \sqrt{k_s^2 - k^2}} + \frac{-(2k^2 - k_s^2)^2}{8k^2 \sqrt{k_d^2 - k^2} (\sqrt{k_s^2 - k^2})^3}, \end{aligned} \quad (8)$$



where  $j$  is the iteration number of the algorithm. After every iteration  $j$ , the new estimate of  $k_s$  can be inserted back into equation (1) or (2) to test for convergence. This numerical process is applied to each specific Lamb wave at each measurement frequency and the result is an estimate of the square of the shear wavenumber. Finally, equation (3) is used to find the shear wavespeed.

Equations (1) – (8) illustrate that if the propagation wavenumber of any wave is known (or can be measured) with the dilatational wavespeed, the shear wavespeed can be estimated. That is, given  $k$  and  $k_d$ , the Newton-Raphson technique can be employed to solve for  $k_s$ . The process will be demonstrated with a numerical simulation and with experimental measurements.

### 3. NUMERICAL SIMULATION

The technique is first applied to a simulated data set created using a fully elastic three-dimensional model of the plate. The model is formulated from Naviers' equations of motion in an isotropic solid. By modeling the response as a sum of a dilatational component and a shear component, the general form of the solutions to the displacement fields are determined. Once these are known, they are inserted into the stress equations on free surfaces of the plate. In the chosen Cartesian coordinate system, the orientation is such that the  $xy$ -plane lies in the major dimensions of the plate and the  $z$ -axis is normal to the plate. On one side of the plate ( $z = 0$ ), the normal stress of the plate is set equal to the stress applied by a point forcing function and this corresponds to a mechanical shaker located at  $x_0$  and  $y_0$ . This equation is written as

$$\sigma_{zz}(x, y, 0, t) = F_0 \delta(x - x_0) \delta(y - y_0) \exp(i\omega t). \quad (9)$$

The other two shear stress boundary conditions at  $z = 0$  are set equal to zero, i.e.,

$$\sigma_{xz}(x, y, 0, t) = 0 \quad (10)$$

and

$$\sigma_{yz}(x, y, 0, t) = 0. \quad (11)$$

On the other side of the plate ( $z = h$ ), all of the stress boundary conditions are zero, and these expressions are written as

$$\sigma_{zz}(x, y, h, t) = 0, \quad (12)$$

$$\sigma_{xz}(x, y, h, t) = 0, \quad (13)$$

and

$$\sigma_{yz}(x, y, h, t) = 0. \quad (14)$$

This produces a linear system of six equations that can be written in matrix form and consist of a dynamics matrix, an unknown coefficient vector, and a load vector. From this, the solution to the unknown constants can be determined. Finally, inserting these unknown values

back into the displacement fields yields a known solution to the displacement fields in all three directions.<sup>12</sup>

The simulation model corresponds to measurements of the normal velocity of the plate (at  $z = h$ ) divided by the input force (at  $z = 0$ ) (the mobility of the system.) in the  $k_x, k_y$  wavevector domain is written as

$$\frac{\dot{W}(k_x, k_y, \omega)}{F_0} = -X_1 i \alpha \omega \sin(\alpha h) + X_2 i \alpha \omega \cos(\alpha h) + X_3 k_y \omega \cos(\beta h) + X_4 k_y \omega \sin(\beta h) - X_5 k_x \omega \cos(\beta h) - X_6 k_x \omega \sin(\beta h), \quad (15)$$

where  $k_x$  is wavenumber with respect to the  $x$ -axis  $\text{rad m}^{-1}$ ,  $k_y$  is wavenumber with respect to the  $y$ -axis  $\text{rad m}^{-1}$ ,  $i$  is  $\sqrt{-1}$ , and

$$\alpha = \sqrt{k_d^2 - k_x^2 - k_y^2} \quad (16)$$

and

$$\beta = \sqrt{k_s^2 - k_x^2 - k_y^2}. \quad (17)$$

The constants  $X_1$  through  $X_6$  are wave propagation coefficients and are determined by solving the three-dimensional elastic plate equation of motion when excited by a point force. This solution was previously developed and is presented in appendix B. It is noted here that geometrical shapes other than a plate will support different wave pattern responses.<sup>15</sup>

Using equation (15), the mobility of the plate in the  $k_x, k_y$  wavevector domain is simulated using a set of parameters that nominally corresponds to the experimental values in the next section. These parameters are dilatational wavespeed of  $1422(1-0.05i) \text{ ms}^{-1}$ , shear wavespeed of  $220(1-0.05i) \text{ ms}^{-1}$ , thickness of  $0.0254 \text{ m}$ , and density of  $1100 \text{ kg m}^{-3}$ . Note that the dilatational and shear wavespeeds are complex; this effect adds structural damping to the analysis that makes the simulation more realistic. Once the mobility fields are created (or later measured), they are

searched so that the relative maximum of each Lamb wave propagating at a specific frequency is identified. From equation (B-35), a relative maxima for each specific wave in the  $k_x, k_y$  wavevector domain can be modeled as a circle centered at  $k_x = k_y = 0$ . Hence, a circular function was fit to the data sets of the relative maxima points. For each specific Lamb wave and fixed frequency, the radius of the circle was determined by the mean value of the radius of all of the individual points, via an ordinary least-square estimator. The resulting radius of the circle is the measured wavenumber  $k$  for the specific Lamb wave identified. Once known, either equation (5) (for symmetric waves) or equation (7) (for antisymmetric waves) is used to estimate the square of the shear wavenumber  $k_s^2$ . From this, the shear wavespeed can be computed.

The simulation was conducted from 1 – 6 kHz in increments of 1 kHz. It is noted at this point that different authors use different terminology to identify individual Lamb waves in the wavevector-frequency (or wavenumber-frequency) plane. In this report, the work of Achenbach<sup>16</sup> was used to define the names of each of the individual waves. Figure 3 is a plot of the wave propagation locations in the  $k_x, k_y$  wavevector domain at 5 kHz. The (first) flexural wave F(0) is denoted with an x, the longitudinal wave L(0) is denoted with a +, the (second) flexural wave FE(1) is denoted with an o, and the circles fit to the markers are denoted with solid lines. (For clarity, the markers have been decimated by 80%.) Once the propagation wavenumbers are known, the shear wavespeed can be estimated using equation (1) for the symmetric L(0) longitudinal wave or equation (2) for the antisymmetric F(0) and FE(1) flexural waves. The results of this simulation are shown in table 1 for six frequency values. The average of the shear wavespeed estimate for the 11 simulated measurements was  $220.5 \text{ ms}^{-1}$ . It is noted that the addition of structural damping produces a slight biasing of the estimated shear wave values for each individual wave. When the damping value was set to 0, the estimation process produced an average value of  $219.9 \text{ ms}^{-1}$ , which varies slightly from the value of  $220 \text{ ms}^{-1}$ , and likely only due to discretization of the simulation in the wavevector domain.



**Table 1. Estimated Shear Wavespeeds for Simulated Waves**

<b>Wave Name and Symmetry</b>	<b>Frequency <math>f</math> (kHz)</b>	<b>Simulated <math>k</math> (rad m<sup>-1</sup>)</b>	<b>Estimated <math>k_s</math> (rad m<sup>-1</sup>)</b>	<b>Estimated <math>c_s</math> (ms<sup>-1</sup>)</b>
F(0) - Antisymmetric	1	50.4	28.4	221.2
F(0) - Antisymmetric	2	79.5	56.8	221.3
F(0) - Antisymmetric	3	107.2	85.1	221.5
F(0) - Antisymmetric	4	134.5	113.1	222.1
F(0) - Antisymmetric	5	161.9	141.1	222.6
L(0) - Symmetric	3	46.4	87.0	216.7
L(0) - Symmetric	4	64.5	115.1	218.4
L(0) - Symmetric	5	86.8	143.0	219.7
L(0) - Symmetric	6	118.5	171.2	220.2
FE(1) - Antisymmetric	5	34.8	141.6	221.8
FE(1) - Antisymmetric	6	62.7	171.7	219.5

The initial estimate of the shear wavespeed is important for convergence of the algorithm. For the FE(1) flexural wave in a plate, the cut-on frequency can be approximated with<sup>12</sup>

$$f_1 \cong \frac{c_s}{2h}, \quad (18)$$

where  $f_1$  is the cut-on frequency (Hz) where the FE(1) wave propagation initiates at zero wavenumber. This simulation shows that the FE(1) wave does not exist at 4 kHz and does exist at 5 kHz, which produces a minimum shear wavespeed value of 203 ms<sup>-1</sup> and a maximum shear wavespeed value of 254 ms<sup>-1</sup> using equation (18). Based on these values, a convergence search using initial estimates from 170 ms<sup>-1</sup> to 270 ms<sup>-1</sup> was conducted. The results are shown in figure 4, where the convergence of each of the eleven simulated waves was tested with respect to varying initial estimates. The initial wavespeed estimate is shown on the x-axis of the plot and the eleven specific waves are depicted on the y-axis of the plot. Each wave is separated by a horizontal dotted line. In figure 4, the black areas indicate nonconvergence and the white areas indicate convergence of the algorithm. The actual wavespeed used to formulate the simulation is shown as a vertical dashed line. Note that the algorithm converges for ten of the eleven simulations with reasonable initial estimates of the shear wavespeed. For the 6 kHz L(0) longitudinal wave, convergence was problematic. Investigation of equation (1) revealed a response with an extremely narrow minimum; thus, the algorithm had difficulty converging on this specific value.

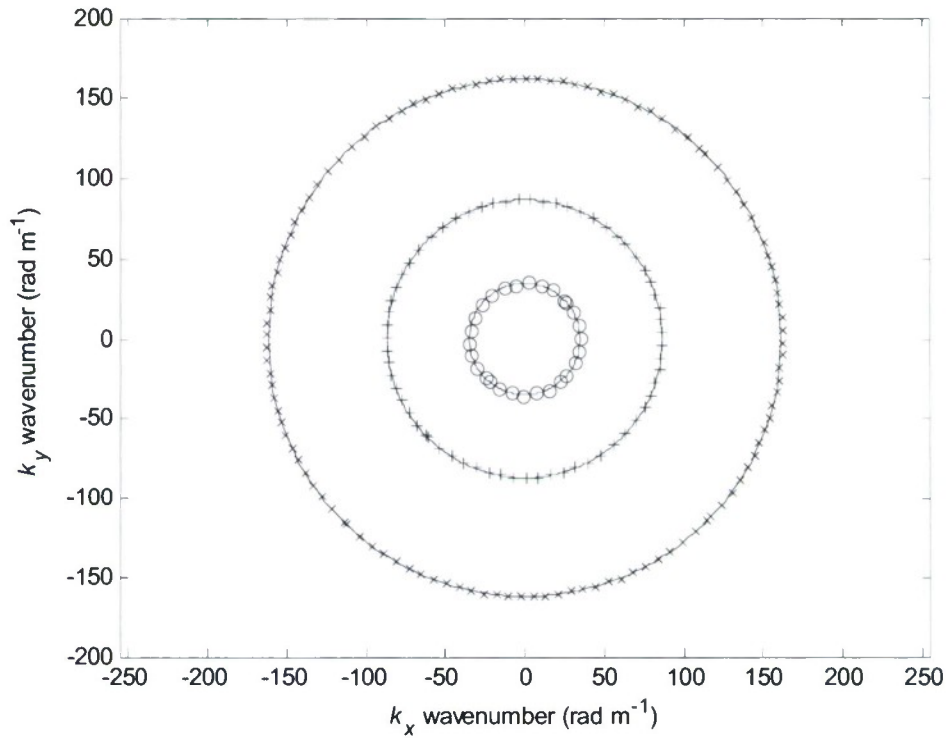


**Figure 3. Locations in the Wavevector Plane for Simulation of  $F(0)$ ,  $L(0)$  and  $FE(1)$  Waves for 5 kHz ( $FE(1)$  Wave (o),  $L(0)$  Wave (+),  $F(0)$  Wave (x), and Least-Square Fit Circles (\_\_\_\_))**

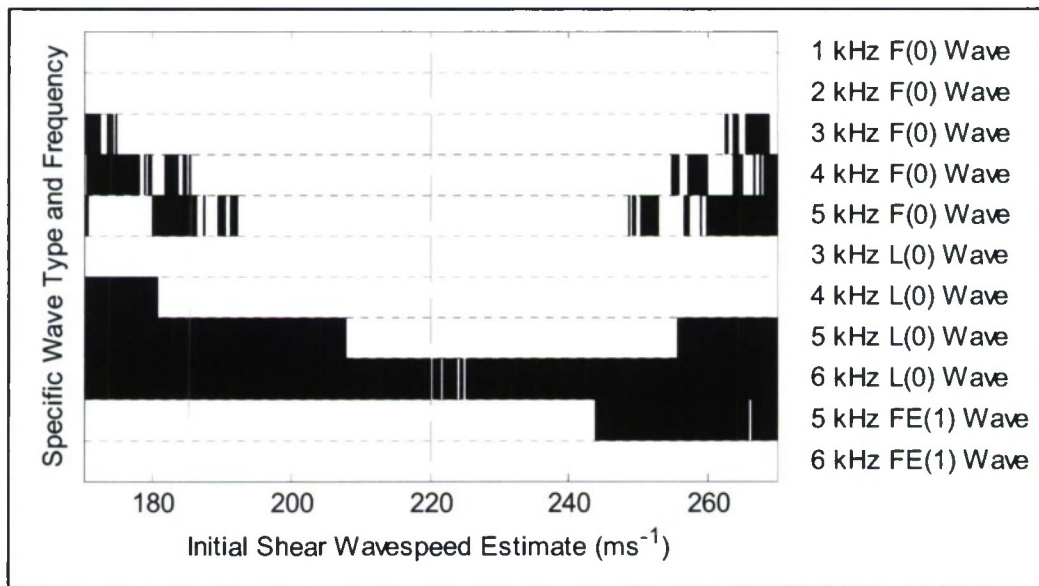


**Figure 4. Performance of Estimation Routine Versus Initial Estimate of Shear Wavespeed for Specific Wave Type and Frequency**

(Black areas indicate nonconvergence and white areas indicate convergence of the algorithm.  
Actual shear wavespeed denoted with a vertical dashed line.)

#### 4. EXPERIMENT

An experiment was undertaken to verify the proposed technique to measure shear wavespeed in a plate. The estimation process uses the following assumption: (1) The return energy from the reflections at the edge of the plate is not interfering with the measurement process, and (2) the particle motion is linear. A plate was molded using Cytech Industries EN-6, a two-part urethane that consists of a mixture of a prepolymer and a curing agent. The plate was 0.780 m by 0.755 m by 0.0254-m thick and weighed 16.6 kg. The dilatational wavespeed was previously measured at  $1421 \text{ ms}^{-1}$ , as described in appendix A. The plate was mounted on four corners with bungee cords and a Wilcoxon Model F3/Z602WA electromagnetic shaker was attached to the back near the middle. When the shaker was turned on, the front side was interrogated with a scanning Polytec LDV PSV-200 Doppler laser vibrometer that measured the normal velocity of the plate. (The experimental setup is shown in figure 5.) The experiment was conducted at a room temperature of  $15.5^\circ\text{C}$ . A square grid of 90 by 90 points with a point-to-point spacing of 0.0082 m was used to collect 8100 spatial domain data points. After the data were collected, they were transformed into the frequency domain using a fast Fourier transform. Next, it was zero padded and transformed into the  $k_x, k_y$  wavevector domain using a two-dimensional 512 by 512 point fast Fourier transform. Once this was accomplished, three Lamb waves were identified based on their relative maxima. Isotropic elastic plate theory predicts that every wave will be circular in the  $k_x, k_y$  wavevector domain; thus, a circle was fit using an ordinary least-square estimate to the wavevector domain data. Measurements were made from 1 to 6 kHz in increments of 1 kHz.

Figure 6 is a plot of the wave propagation locations in the  $k_x, k_y$  wavevector domain at 5 kHz. The F(0) flexural wave data are denoted with an x, the L(0) longitudinal wave data are denoted with a +, the FE(1) flexural wave is denoted with an o, and the circles fit to the markers are denoted with solid lines. For clarity, the markers have been decimated by 80%. Once the propagation wavenumbers are known, the shear wavespeed can be estimated using equation (1) for the symmetric L(0) longitudinal wave or equation (2) for the antisymmetric F(0) and FE(1) flexural waves. (Note, at the frequency of 5 kHz, the F(0) flexural wave is beginning to become

incoherent across the major dimensions of the plate.) The results of this estimation procedure are shown in table 2 for all of the waves measured during the test and at all experimental frequencies. (The measured propagation wavenumber of the L(0) longitudinal and F(0) flexural waves at 4 kHz were used to construct figures 1 and 2, respectively.) The average value for the shear wavespeed estimate for the F(0) flexural wave was  $235.6 \text{ ms}^{-1}$ , the average shear wavespeed estimate for the L(0) longitudinal wave was  $206.5 \text{ ms}^{-1}$ , and the average value shear wavespeed estimate for the FE(1) flexural wave was  $211.9 \text{ ms}^{-1}$ . This indicates a mild dispersion of the shear wavespeed with respect to wave type. The average shear wavespeed for all measurements was  $220.7 \text{ ms}^{-1}$ . Using this average value and the value of the dilatational wavespeed, the dispersion curve in the wavenumber-frequency plane can be calculated. This is displayed as figure 7 along with each data point. The slight mismatch between theory and experiment is due to the variation of the shear wavespeed with respect to each individual wave.

**Table 2. Estimated Shear Wavespeeds for All Measured Waves**

<b>Wave Name and Symmetry</b>	<b>Frequency <math>f</math> (kHz)</b>	<b>Simulated <math>k</math> (rad m<sup>-1</sup>)</b>	<b>Estimated <math>k_s</math> (rad m<sup>-1</sup>)</b>	<b>Estimated <math>c_s</math> (ms<sup>-1</sup>)</b>
F(0) - Antisymmetric	1	49.2	26.5	229.9
F(0) - Antisymmetric	2	75.8	53.0	237.3
F(0) - Antisymmetric	3	103.0	80.7	233.6
F(0) - Antisymmetric	4	128.9	107.3	234.2
F(0) - Antisymmetric	5	150.3	129.2	243.2
L(0) - Symmetric	3	50.4	93.6	201.3
L(0) - Symmetric	4	68.9	121.3	207.1
L(0) - Symmetric	5	94.4	150.9	208.2
L(0) - Symmetric	6	131.0	180.0	209.5
FE(1) - Antisymmetric	5	41.7	148.4	211.8
FE(1) - Antisymmetric	6	67.8	177.8	212.0



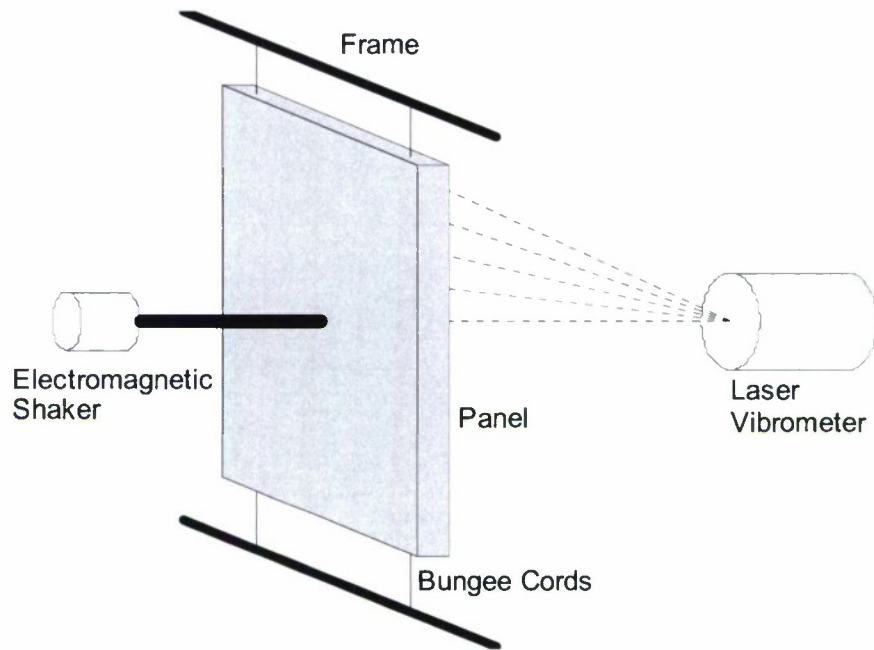


**Figure 5. Experimental Setup of the Shear Wave Estimation Test**

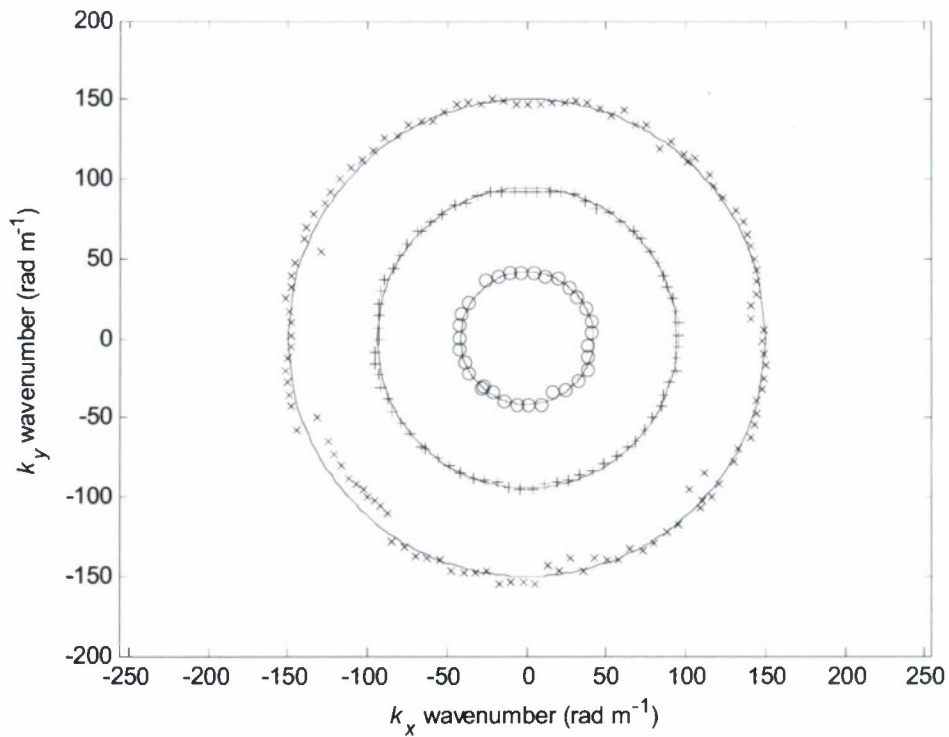


**Figure 6. Locations in the  $k_x, k_y$  Wavevector Plane for Experiment of  $F(0)$ ,  $L(0)$  and  $FE(1)$  Waves for 5 kHz ( $FE(1)$  Wave (o),  $L(0)$  Wave (+),  $F(0)$  Wave (x), and Least-Square Fit Circles ( \_\_\_\_ ))**

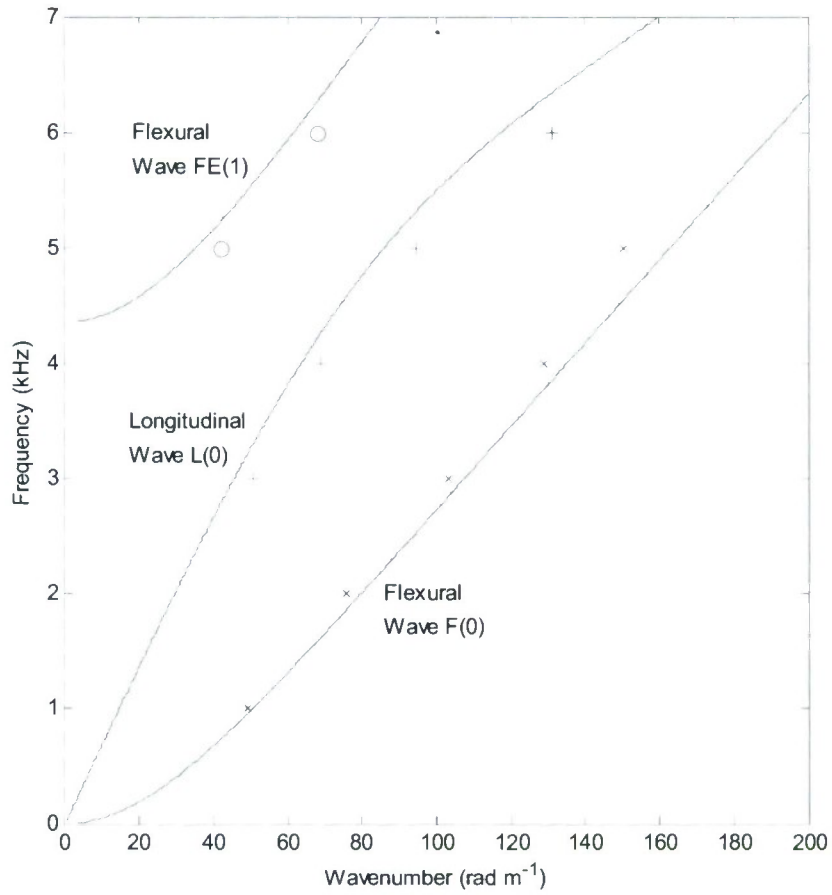


**Figure 7. Dispersion Curve of the Plate F(0) Wave Data (x), L(0) Wave Data (+), FE(1) Wave Data (o), and Theory ( \_\_\_\_ )**

Several parameters were varied to examine the accuracy of the measurement technique. First, the dilatational wavespeed was halved to  $710.5 \text{ ms}^{-1}$  and then doubled  $2840 \text{ ms}^{-1}$ , which produced average shear wavespeed estimates of  $224.1 \text{ ms}^{-1}$  and  $220.0 \text{ ms}^{-1}$ , respectively. This shows conclusively that the shear wavespeed estimate is relatively invariant to the dilatational wavespeed. Second, the thickness of the plate was thinned by 10% to  $0.0229 \text{ m}$  and thickened by 10% to  $0.0279 \text{ m}$ , and this produced average shear wavespeed estimates of  $220.3 \text{ ms}^{-1}$  and  $222.0 \text{ ms}^{-1}$ , respectively. Finally, each of the measurements was statistically analyzed by calculating the standard deviation of the radius of the data points for each wave at every frequency. Once known, the shear wavespeeds were estimated at +1 and -1 standard deviation away from the mean. The results are shown for each individual wave in table 3. At -1 standard deviation, the average shear wavespeed was estimated to be  $229.9 \text{ ms}^{-1}$ , and for +1 standard

deviation, the average shear wavespeed was estimated to be  $213.0 \text{ ms}^{-1}$ . These estimates are off by the original estimate of  $220.7 \text{ ms}^{-1}$  by 4.4% and 3.3%, respectively, which generally indicates a stable estimation process.

**Table 3. Statistical Analysis of Estimated Shear Wavespeeds**

<b>Wave Name and Symmetry</b>	<b>Frequency <math>f</math> (kHz)</b>	<b>Standard Deviation (<math>\text{rad m}^{-1}</math>)</b>	<b>Estimated <math>c_s</math> (-1 Std. Dev.) (<math>\text{m s}^{-1}</math>)</b>	<b>Estimated <math>c_s</math> (+1 Std. Dev.) (<math>\text{m s}^{-1}</math>)</b>
F(0) - Antisymmetric	1	3.6	261.2	204.8
F(0) - Antisymmetric	2	3.3	253.3	223.1
F(0) - Antisymmetric	3	2.6	241.7	226.0
F(0) - Antisymmetric	4	2.2	239.3	229.3
F(0) - Antisymmetric	5	4.3	251.9	235.2
L(0) - Symmetric	3	3.0	212.5	191.3
L(0) - Symmetric	4	2.9	214.3	200.8
L(0) - Symmetric	5	1.2	209.9	206.7
L(0) - Symmetric	6	2.3	215.9	207.7
FE(1) - Antisymmetric	5	1.6	214.1	209.4
FE(1) - Antisymmetric	6	2.0	214.9	209.2

## 5. CONCLUSIONS

The shear wavespeed of an isotropic plate can be accurately estimated using the measurement technique developed in this report. The approach consists of exciting the plate with a point force, measuring the normal component of velocity over its surface, and transforming the spatial measurements into the  $k_x, k_y$  wavevector domain. The described technique is enabled by high-resolution wavevector measurement (via a scanning laser Doppler vibrometer). This fine resolution, coupled with zero padding within the  $k_x, k_y$  spectra, allows for straightforward identification of propagating Lamb waves and their associated wavenumbers. An estimate of the shear wavespeed, using a Newton-Raphson method applied to the theoretical Rayleigh-Lamb plate equations, is straightforward. Numerical simulations and experimental measurements demonstrated that the method provides accurate estimates of the shear wavespeed, even when other measurement parameters have uncertainties. Nonconvergence of the Newton-Raphson method can occur, primarily due to poor initial estimates of the shear wavespeed, although this did not occur with the experimental data evaluated here.



## APPENDIX A

### MEASUREMENT OF DILATATIONAL WAVESPEED

The dilatational wavespeed was measured using an echo reduction test. An echo reduction test is accomplished by insonifying the plate and measuring the transfer function of the incident acoustic energy divided by the reflected acoustic energy. This previously developed estimation method<sup>17</sup> identifies the peaks in the data and relates each specific peak to a corresponding wavelength that is a half integer multiplication of the thickness of the plate. Figure A-1 is the echo reduction data for the EN-6 plate. When the frequencies of the relative maxima are determined, they can be related to the dilatational wavespeed by

$$(c_d)_n = \frac{hf_n}{n}, \quad (\text{A-1})$$

where  $f_n$  is the frequency of the  $n$ th relative maxima (Hz or  $\text{cycles s}^{-1}$ ) and  $n$  is the number of wavelengths in the material that creates the relative maxima (cycles). For the three relative maxima shown in figure A-1, the values of  $n$  are  $1/2$ ,  $1$ , and  $3/2$ , cycles, respectively. Once this relationship is known, the dilatational wavespeed can be calculated. The results are shown in table A-1. The average dilatational wavespeed for the test was calculated to be  $1421 \text{ ms}^{-1}$ . This method was shown to have an average difference of dilatational wavespeed of 1.6% when compared to an inverse method developed using the fully elastic response of the plate.

**Table A-1. Dilatational Wavespeed Estimates at Relative Maxima**

$n$ (cycles)	$f_n$ (kHz)	$(c_d)_n$ (m s <sup>-1</sup> )
1/2	28.3	1435
1	56.0	1422
3/2	83.0	1406

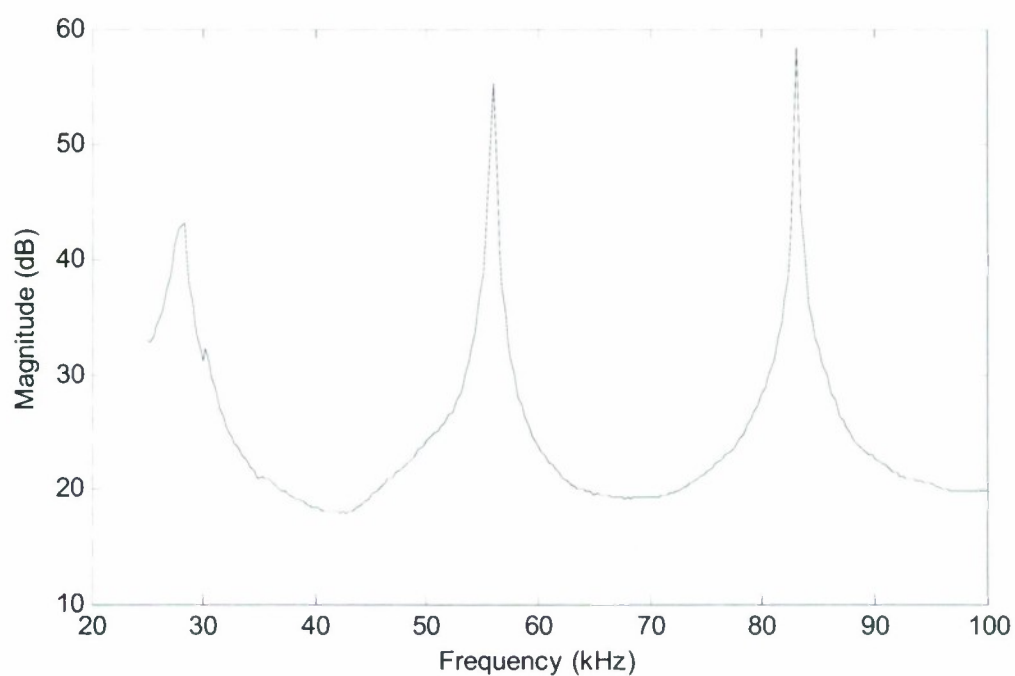


**Figure A-1. Magnitude of the Echo Reduction for the Plate Under Investigation**

## APPENDIX B COEFFICIENTS OF TRANSFER FUNCTION MATRICES

The dynamic model of the plate has been previously developed<sup>12</sup> for a system with no variation in the  $x$ -direction. Because the system described here has a point load (located at  $x_0 = 0$  and  $y_0 = 0$ ), the previous model is extended to include the variation in the  $x$ -direction, as well as retain the variations in the  $y$ - and  $z$ -directions. This theoretical development follows the previous model equations (8.1.62) – (8.1.67)<sup>12</sup> adding this additional degree of freedom.

The constants  $X_1$  through  $X_6$  are wave propagation coefficients and are determined by solving the matrix equation

$$\mathbf{x} = \mathbf{A}^{-1}\mathbf{f}, \quad (\text{B-1})$$

where  $\mathbf{x}$  is a  $6 \times 1$  vector written as

$$\mathbf{x} = \{X_1 \quad X_2 \quad X_3 \quad X_4 \quad X_5 \quad X_6\}^T, \quad (\text{B-2})$$

the nonzero entry of the  $6 \times 1$  vector  $\mathbf{f}$  is

$$f_1 = F_0, \quad (\text{B-3})$$

and the nonzero entries of the  $6 \times 1$  matrix  $\mathbf{A}$  are

$$a_{11} = -\lambda(\alpha^2 + k_x^2 + k_y^2) - 2\mu\alpha^2, \quad (\text{B-4})$$

$$a_{14} = -2i\mu\beta k_y, \quad (\text{B-5})$$

$$a_{16} = 2i\mu\beta k_x, \quad (\text{B-6})$$

$$a_{22} = 2i\mu\alpha k_y, \quad (\text{B-7})$$

$$a_{23} = -\mu(\beta^2 + k_x^2 - k_y^2), \quad (\text{B-8})$$

$$a_{25} = -2\mu k_x k_y, \quad (\text{B-9})$$

$$a_{32} = 2i\mu\alpha k_x, \quad (\text{B-10})$$

$$a_{33} = \mu k_x k_y, \quad (\text{B-11})$$

$$a_{34} = -\mu k_x k_y, \quad (\text{B-12})$$

$$a_{35} = \mu(\beta^2 - k_x^2), \quad (\text{B-13})$$

$$a_{36} = -\mu k_y^2, \quad (\text{B-14})$$

$$a_{41} = -[\lambda(\alpha^2 + k_x^2 + k_y^2) + 2\mu\alpha^2]\cos(\alpha h), \quad (\text{B-15})$$

$$a_{42} = -[\lambda(\alpha^2 + k_x^2 + k_y^2) + 2\mu\alpha^2]\sin(\alpha h), \quad (\text{B-16})$$

$$a_{43} = 2i\mu\beta k_y \sin(\beta h), \quad (\text{B-17})$$

$$a_{44} = -2i\mu\beta k_y \cos(\beta h), \quad (\text{B-18})$$

$$a_{45} = -2i\mu\beta k_x \sin(\beta h), \quad (\text{B-19})$$



$$a_{46} = 2i\mu\beta k_x \cos(\beta h), \quad (\text{B-20})$$

$$a_{51} = -2i\mu\alpha k_y \sin(\alpha h), \quad (\text{B-21})$$

$$a_{52} = 2i\mu\alpha k_y \cos(\alpha h), \quad (\text{B-22})$$

$$a_{53} = -\mu(\beta^2 + k_x^2 - k_y^2) \cos(\beta h), \quad (\text{B-23})$$

$$a_{54} = -\mu(\beta^2 + k_x^2 - k_y^2) \sin(\beta h), \quad (\text{B-24})$$

$$a_{55} = -2\mu k_x k_y \cos(\beta h), \quad (\text{B-25})$$

$$a_{56} = -2\mu k_x k_y \sin(\beta h), \quad (\text{B-26})$$

$$a_{61} = -2i\mu\alpha k_x \sin(\alpha h), \quad (\text{B-27})$$

$$a_{62} = 2i\mu\alpha k_x \cos(\alpha h), \quad (\text{B-28})$$

$$a_{63} = \mu k_x k_y [\cos(\beta h) - \sin(\beta h)], \quad (\text{B-29})$$

$$a_{64} = \mu k_x k_y [\sin(\beta h) - \cos(\beta h)], \quad (\text{B-30})$$

$$a_{65} = \mu(\beta^2 - k_x^2) \cos(\beta h) - \mu k_y^2 \sin(\beta h), \quad (\text{B-31})$$

and

$$a_{66} = \mu(\beta^2 - k_x^2) \sin(\beta h) - \mu k_y^2 \cos(\beta h). \quad (\text{B-32})$$

In the above equations,  $\lambda$  and  $\mu$  are the Lamé constants and are related to the wavespeeds by

$$c_d = \sqrt{\frac{\lambda + 2\mu}{\rho}} \quad (\text{B-33})$$

and

$$c_s = \sqrt{\frac{\mu}{\rho}}, \quad (\text{B-34})$$

where  $\rho$  is the density of the plate ( $\text{kg m}^{-3}$ ). Finally, the wavenumber in the plate is related to the  $k_x$  and  $k_y$  wavenumbers by

$$\kappa = \sqrt{k_x^2 + k_y^2}. \quad (\text{B-35})$$

When the response of the plate is at a wavenumber that corresponds to a Lamb wave, the propagation wavenumber equals the Lamb propagation wavenumber, i.e.,  $\kappa = k$ .

## REFERENCES

1. W. M. Madigosky and G. F. Lee, "Improved Resonance Technique for Materials Characterization," *Journal of the Acoustical Society of America*, vol. 73, no. 4, pp. 1374-1377, 1983.
2. S. O. Oyaniji and G. R. Tomlinson, "Determination of the Complex Moduli of Viscoelastic Structural Elements by Resonance and Non-resonance Methods," *Journal of Sound and Vibration*, vol. 101, no. 3, pp. 277-298, 1985.
3. S. L. Garrett, "Resonant Acoustic Determination of Elastic Moduli," *Journal of the Acoustical Society of America*, vol. 88, no. 1, pp. 210-220, 1990.
4. F. J. Nieves, F. Gascón, and A. Bayón, "Measurement of the Dynamic Elastic Constants of Short Isotropic Cylinders," *Journal of Sound and Vibration*, vol. 265, no. 5, pp. 917-933, 2003.
5. J. L. Buchanan, "Numerical Solution for the Dynamic Moduli of a Viscoelastic Bar," *Journal of the Acoustical Society of America*, vol. 81, no. 6, pp. 1775-1786, 1987.
6. A. J. Hull, "An Inverse Method to Measure the Axial Modulus of Composite Materials Under Tension," *Journal of Sound and Vibration*, vol. 195, no. 4, pp. 545-551, 1996.
7. P.-O. Larsson, "Determination of Young's and Shear Moduli from Flexural Vibrations of Beams," *Journal of Sound and Vibration*, vol. 146, no. 1, pp. 111-123, 1991.
8. S. I. Rokhlin and W. Wang, "Measurements of Elastic Constants of Very Thin Anisotropic Plates," *Journal of the Acoustical Society of America*, vol. 94, no. 5, pp. 2721-2730, 1993.
9. M. Castaings, B. Hosten, and T. Kundu, "Inversion of Ultrasonic, Plane-Wave Transmission Data in Composite Plates to Infer-Viscoelastic Material Properties," *NDT&E International*, vol. 33, no. 6, pp. 377-392, 2000.
10. A. Baltazar, L. Want, B. Xie, and S.I. Rokhlin, "Inverse Ultrasonic Determination of Imperfect Interfaces and Bulk Properties of a Layer Between Two Solids," *Journal of the Acoustical Society of America*, vol. 114, no. 3, pp. 1424-1434, 2003.
11. Y.-T. Cheng and C.-M. Cheng, "Scaling, Dimensional Analysis and Indentation Measurements," *Materials Science and Engineering: R: Reports*, vol. 44, pp. 91-149, 2004.
12. K. F. Graff, *Wave Motion in Elastic Solids*, Dover Publications, New York, 1975.
13. L. M. Brekhovskikh, *Waves in Layered Media*, Academic Press, San Diego, CA, 1980 (original printing 1973).

14. M. C. Potter, *Mathematical Methods in the Physical Sciences*, Prentice-Hall, Inc., Englewood Cliffs, NJ, 1978.
15. E. G. Williams, *Fourier Acoustics*, Academic Press, London, 1999.
16. J. D. Achenbach, *Wave Propagation in Elastic Solids*, Elsevier Science Publishers B.V., Amsterdam, The Netherlands, 1975.
17. G. J. Gartland, C.J. Radcliffe, and A. J. Hull, "Measurement of Dilatational Wave Speed Using an Echo Reduction Test," submitted to *Journal of Sound and Vibration*, 2008.



## INITIAL DISTRIBUTION LIST

Addressee	No. of Copies
Defense Technical Information Center	2
Center for Naval Analyses	1
Michigan State University (J. Beck, C. R. MacCluer)	2